

The telomeric protein TERF2/TRF2 impairs HMGB1-driven autophagy

Sara Iachettini, Fabio Ciccarone, Carmen Maresca, Carmen D' Angelo, Eleonora Petti, Serena Di Vito, Maria Rosa Ciriolo, Pasquale Zizza & Annamaria Biroccio

To cite this article: Sara Iachettini, Fabio Ciccarone, Carmen Maresca, Carmen D' Angelo, Eleonora Petti, Serena Di Vito, Maria Rosa Ciriolo, Pasquale Zizza & Annamaria Biroccio (2023) The telomeric protein TERF2/TRF2 impairs HMGB1-driven autophagy, *Autophagy*, 19:5, 1479-1490, DOI: [10.1080/15548627.2022.2138687](https://doi.org/10.1080/15548627.2022.2138687)

To link to this article: <https://doi.org/10.1080/15548627.2022.2138687>



© 2022 The Author(s). Published by Informa UK Limited, trading as Taylor & Francis Group.



[View supplementary material](#)



Published online: 30 Oct 2022.



[Submit your article to this journal](#)



Article views: 3920



[View related articles](#)



[View Crossmark data](#)



Citing articles: 13 [View citing articles](#)

The telomeric protein TERF2/TRF2 impairs HMGB1-driven autophagy

Sara Iachettini^{a*}, Fabio Ciccarone^{b,c*}, Carmen Maresca^a, Carmen D' Angelo^a, Eleonora Petti^a, Serena Di Vito^a, Maria Rosa Ciriolo^{b,c}, Pasquale Zizza^{a*,†}, and Annamaria Biroccio^{a*,†}

^aTranslational Oncology Research Unit, IRCCS - Regina Elena National Cancer Institute, Rome, Italy; ^bDepartment of Biology, University of Rome "Tor Vergata", Rome, Italy; ^cBiochemistry of aging section, IRCCS San Raffaele Roma, Rome, Italy

ABSTRACT

TERF2/TRF2 is a pleiotropic telomeric protein that plays a crucial role in tumor formation and progression through several telomere-dependent and -independent mechanisms. Here, we uncovered a novel function for this protein in regulating the macroautophagic/autophagic process upon different stimuli. By using both biochemical and cell biology approaches, we found that TERF2 binds to the non-histone chromatin-associated protein HMGB1, and this interaction is functional to the nuclear/cytoplasmic protein localization. Specifically, silencing of TERF2 alters the redox status of the cells, further exacerbated upon EBSS nutrient starvation, promoting the cytosolic translocation and the autophagic activity of HMGB1. Conversely, overexpression of wild-type TERF2, but not the mutant unable to bind HMGB1, negatively affects the cytosolic translocation of HMGB1, counteracting the stimulatory effect of EBSS starvation. Moreover, genetic depletion of HMGB1 or treatment with inflachromene, a specific inhibitor of its cytosolic translocation, completely abolished the pro-autophagic activity of TERF2 silencing. In conclusion, our data highlighted a novel mechanism through which TERF2 modulates the autophagic process, thus demonstrating the key role of the telomeric protein in regulating a process that is fundamental, under both physiological and pathological conditions, in defining the fate of the cells.

Abbreviations: ALs: autolysosomes; ALT: alternative lengthening of telomeres; ATG: autophagy related; ATM: ATM serine/threonine kinase; CQ: Chloroquine; DCFDA: 2',7'-dichlorofluorescein diacetate; DDR: DNA damage response; DHE: dihydroethidium; EBSS: Earle's balanced salt solution; FACS: fluorescence-activated cell sorting; GFP: green fluorescent protein; EGFP: enhanced green fluorescent protein; GSH: reduced glutathione; GSSG: oxidized glutathione; HMGB1: high mobility group box 1; ICM: inflachromene; IF: immunofluorescence; IP: immunoprecipitation; NAC: N-acetyl-L-cysteine; NHEJ: non-homologous end joining; PLA: proximity ligation assay; RFP: red fluorescent protein; ROS: reactive oxygen species; TIF: telomere-induced foci; TERF2/TRF2: telomeric repeat binding factor 2.

ARTICLE HISTORY

Received 11 April 2022
Revised 13 Oct 2022
Accepted 17 October 2022

KEYWORDS

Autophagy; cancer; cell biology; HMGB1; oxidative stress; ROS; TERF2/TRF2

Introduction

TERF2/TRF2 (telomeric repeat binding factor 2) is a component of the Shelterin multiprotein complex that is essential to inhibit ATM (ATM serine/threonine kinase) signaling and non-homologous end joining repair pathway at the end of chromosomes, thus preserving telomere integrity and genome stability [1,2].

TERF2 has also been found overexpressed in several tumors [3–7] and promotes tumor formation and progression [8–11]. The involvement of TERF2 in tumorigenesis relies not only on its telomeric roles but also on several non-canonical functions. Interestingly, TERF2 can regulate gene expression through the binding to the interstitial telomeric sequences dispersed in the genome [12,13], thus affecting several biological processes involved in tumorigenesis, included immune response [14,15] and angiogenesis [16,17]. Recently, we revealed that pro-tumoral activity of TERF2 also goes through the control of the microRNAs (miRNAs) expression, so

defining a new mechanism through which TERF2 can affect the expression and the function of several target proteins [18].


At the structural level, TERF2 is characterized by multiple domains mediating its interaction with DNA and other proteins. In particular, TERF2 can act as a hub for both telomeric and non-telomeric binding partners, thus promoting their localization on the DNA [19]. Despite the increasing knowledge about TERF2 activity, a number of processes regulated by this protein are still under investigation. Here we identified a novel non-canonical role of TERF2 in controlling macroautophagy/autophagy.

Autophagy is an intracellular catabolic pathway playing a fundamental role in removing unnecessary or dysfunctional cellular components (*e.g.* misfolded or aggregated proteins, nucleic acids fragments and damaged organelles) through their inclusion within autophagosomes that, fusing with lysosomes, originates the autolysosomes (ALs), acidic vesicular organelles aimed at the digestion of the sequestered material

CONTACT Pasquale Zizza  pasquale.zizza@ifo.it; Annamaria Biroccio  annamaria.biroccio@ifo.it  Translational Oncology Research Unit, Regina Elena National Cancer Institute, Via Elio Chianesi, 53 - 00186 Roma, Italy

*These authors contributed equally to this work.

†These authors contributed equally to this work

 Supplemental data for this article can be accessed online at <https://doi.org/10.1080/15548627.2022.2138687>

© 2022 The Author(s). Published by Informa UK Limited, trading as Taylor & Francis Group.

This is an Open Access article distributed under the terms of the Creative Commons Attribution-NonCommercial-NoDerivatives License (<http://creativecommons.org/licenses/by-nc-nd/4.0/>), which permits non-commercial re-use, distribution, and reproduction in any medium, provided the original work is properly cited, and is not altered, transformed, or built upon in any way.

[20]. Even if constitutively active under basal conditions in several cell types, the autophagic process is additionally enhanced by a large array of cellular stresses, such as nutrient deprivation, hypoxia, DNA damage and oxidative stress, thus functioning – in a context-dependent way – as a self-nourishment or a homeostasis maintenance process [21]. As such, activation of autophagy associates with both physiological and pathological conditions, such as cancer [22].

Notably, the role of autophagy in cancer is dual since it acts as a tumor suppressor during the initial stages, then evolving into a tumor promoting response in concomitance with the progression of the malignancy [23]. Moreover, autophagy has been demonstrated to sustain the viability of well-established tumors by acting as a resistance mechanism to cytotoxic agents, thus representing an obstacle for successful patients' treatment [24].

At the mechanistic level, autophagy is primarily controlled by members of the ATG (autophagy related) protein family [25]. However, in the last few years a number of novel autophagic players have been identified [26]. Among these, HMGB1 – a member of the high mobility group (HMG) protein family – has been abundantly investigated. First identified in the early 1970s as a non-histone chromatin-associated protein, HMGB1 is a widely-expressed and highly-abundant nuclear factor acting as a DNA chaperone involved in the regulation of replication, transcription, recombination and repair [27]. Together with its nuclear functions, HMGB1 has been reported to act as a sensor protein that, upon stress conditions, translocates from the nucleus to the cytosol and, eventually, exits out of the cell [28]. Interestingly, the cytosolic HMGB1, through its interaction with BECN1 (beclin 1), promotes the autophagic process [29].

Among the mechanisms that can regulate HMGB1-dependent autophagy, oxidative stress has been reported to play a key role [28,30]. Indeed, the unbalance between the production of reactive oxygen species (ROS) and antioxidant defenses – arising under this stress condition – promotes the oxidation of specific aminoacidic residues of HMGB1, necessary for the proper localization of HMGB1 in the cytosol and, consequently, for promoting the autophagic activity of the protein [30,31].

Here, we found that the mechanism through which TERF2 regulates autophagy is dependent on its capability to control the cytosolic translocation of HMGB1. This would represent an additional mechanism through which TERF2, besides its well-known involvement in activating DNA damage response, can affect the autophagic process in cancer cells. Overall, being autophagy a key event in tumor formation and progression, our data contribute to extend the current knowledge concerning the complex and multifaceted roles of TERF2 in cancer biology.

Results

HMGB1 interacts with TERF2 in the nucleus

Based on a previous paper from our group [32], showing that HMGB1 localizes at telomeres, here, we wondered if it could interact with TERF2, which is known to function as

a telomeric hub for protein complexes. Immunofluorescence (IF) confocal microscopy experiments evidenced that HMGB1 colocalizes with TERF2 in both telomerase-positive human cervical cancer cells, HeLa (Figure 1(a); Fig S1A), and alternative lengthening of telomeres (ALT)-positive human osteosarcoma cells, U2OS (Fig. S1A and S1B). In addition, immunoprecipitation (IP) experiments demonstrated that the two proteins reciprocally interact (Figure 1(b); Fig. S1C). To directly visualize this interaction in cells, a proximity ligation assay (PLA) – an experimental tool that allows to visualize *in-situ* co-localizations between proteins distant less than 40 nm – was performed. Quantification of PLA spots by deconvolution microscopy revealed that TERF2 overexpression (pTERF2) significantly increases the number of colocalizations (Figure 1(c)), while its silencing (shTERF2), as well as the interference of HMGB1, decreases the PLA signal visualized in the nuclei of the cells (Fig. S1D and S1E).

To gain deeper insight into the mechanism of this interaction, affinity-isolation experiments were performed by using recombinant TERF2-conjugated beads. Notably, the assay demonstrated that TERF2 is unable to precipitate HMGB1 (Fig. S1F), suggesting that DNA can mediate the interaction between the two proteins. In agreement with this hypothesis, IP experiments evidenced a loss of the interaction upon the enzymatic digestion of the DNA (Fig. S1G). To confirm and reinforce these results, HeLa cells were transiently transfected with a mutant of TERF2 (pTERF2 Δ C) that, lacking the Myb-domain at the C terminus, is unable to bind the DNA [33]. Notably, the TERF2 Δ C mutant, in contrast with its wild-type counterpart (pTERF2), did not immunoprecipitate HMGB1 (Figure 1(d)), definitively proving the essential role played by the DNA in mediating this interaction.

TERF2 retains HMGB1 into the nucleus

Starting from these results, we decided to investigate the functional relevance of the interaction between TERF2 and HMGB1. In particular, being the functions of HMGB1 tightly dependent on its cellular localization [28], we questioned if TERF2 might affect the shuttling of HMGB1 from the nucleus to the cytosol. To address this point, HeLa cells, chronically silenced for TERF2 (shTERF2), and their control counterpart (shSCR), were transfected with enhanced green fluorescent protein (EGFP)-tagged HMGB1 (EGFP-HMGB1) and the cellular localization of the exogenous protein was evaluated. Interestingly, IF experiments (Figure 2(a)) – then biochemically confirmed by western blotting (WB) analyses (Figure 2(b)) – demonstrated that the silencing of TERF2 determines a significant increase in the cytosolic translocation of HMGB1, and this effect is maintained upon EBSS starvation, a pro-autophagic stimulus that promotes the release of HMGB1 out of the nucleus [29] (Figures 2(a-b)). To strengthen our data, mirror experiments were performed in cells overexpressing TERF2. The obtained data evidenced that the upregulation of the protein negatively affects the cytosolic translocation of HMGB1, counteracting the stimulatory effect of EBSS starvation (Fig. S2A and S2B). For completeness, all these data were also confirmed in cells subjected to transient modulation of TERF2 expression (Figure 2(c); Fig. S2C-S2E). Conversely to the overexpression of the wild-type form of TERF2, the expression of the TERF2 Δ C mutant does not inhibit the cytosolic translocation of

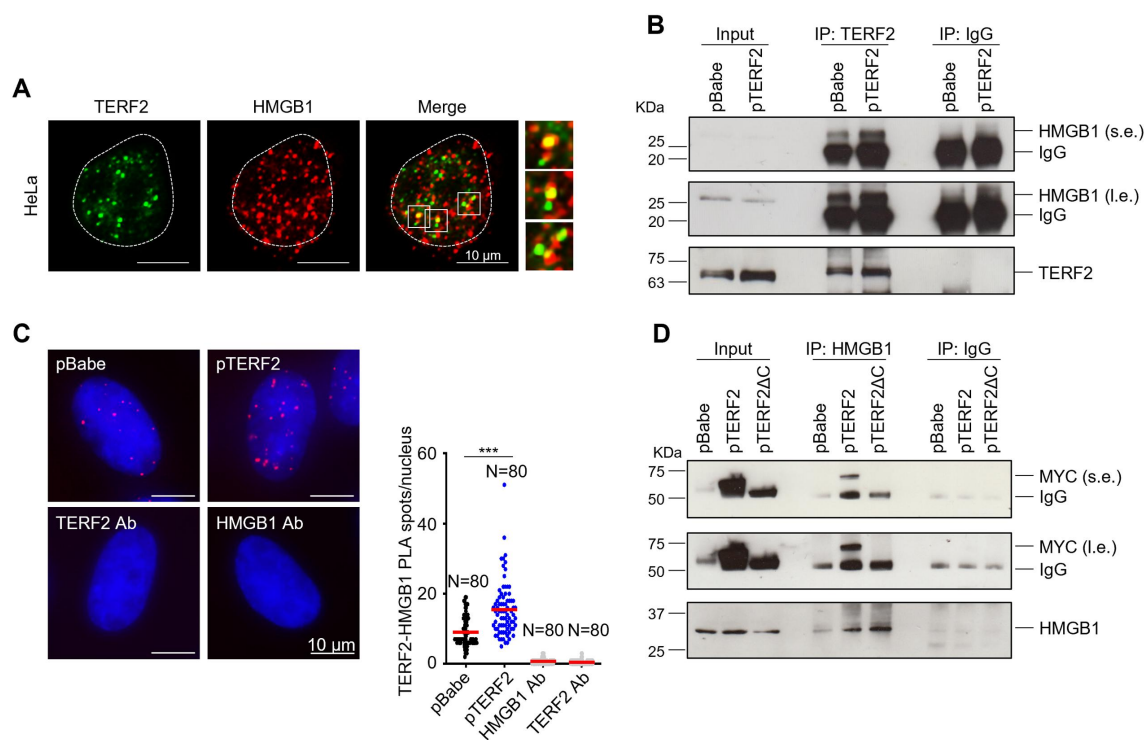


Figure 1. HMGB1 interacts with the telomeric protein TERF2. (A) Representative images of co-immunofluorescence experiments performed in human cervical cancer cells (HeLa) using the antibodies against TERF2 (green spots) and HMGB1 (red spots). The nuclei were stained with DAPI (blue). The images were acquired by confocal microscopy (63X magnification). Colocalization enlargements are shown. (B) Immunoprecipitation (IP) experiment performed with nuclear extracts obtained from HeLa cells subjected (pTERF2) or not (pBabe) to stable overexpression of TERF2. IP were performed by using an antibody against TERF2. The amount of HMGB1 immunoprecipitated by TERF2 antibody was evaluated by western blot analysis. The evaluation of TERF2 levels were used as immunoprecipitation control. (C) Proximity ligation assay (PLA) performed in HeLa pBabe and pTERF2 cells by using the antibodies against TERF2 and HMGB1. The red signals indicate the proximity of the indicated proteins. In all sections, the nuclei were stained with DAPI (blue). As a negative control, each antibody was used alone. *Left panel.* Representative images acquired by deconvolution microscopy (63X magnification). *Right panel.* Quantitative analysis performed counting the number of TERF2-HMGB1 PLA spots for nucleus (N = 80 cells). (D) IP experiment performed in HeLa cells overexpressing the MYC-tagged form of the wild-type (pTERF2) or mutant (pTERF2 Δ C) TERF2. IP were performed by using an antibody against HMGB1. The cells expressing the pBabe empty vector (pBabe) were used as the control counterpart. The amount of TERF2 immunoprecipitated by HMGB1 antibody was evaluated by western blot analysis by using an antibody against MYC. HMGB1 protein levels were used as immunoprecipitation control. Input lanes show the signal relative to the endogenous MYC (first lane, pBabe), exogenous MYC-tagged TERF2 (second lane, pTERF2) and exogenous MYC-tagged truncated TERF2 mutant (third lane, pTERF2 Δ C). As reported in the figure, IgG signals are visible in the IP lanes. Dot plot represents the mean values \pm S.D. of three independent experiments. *** $p < 0.001$.

HMGB1, confirming that the localization of the protein depends on its interaction with TERF2 (Fig. S2D and S2E). Since the telomeric protein TERF1/TRF1 is known to share with TERF2 the binding sites at telomeres, other than a number of biological functions, we finally evaluated the capability of this telomeric protein to interact with HMGB1 and to affect – similar to TERF2 – its shuttling from the nucleus to the cytosol.

Interestingly, IP experiments demonstrated that HMGB1 – even localizing at telomeres [32] – does not interact with TERF1 (Figure 2(d)). This result is tightly in line with the IF experiments showing that silencing of TERF1 is unable to promote the cytosolic translocation of HMGB1 (Figure 2(c); Fig. S2C), confirming the specificity of the TERF2 in controlling the cellular localization of HMGB1.

TERF2 regulates autophagy by modulating HMGB1 localization

Cytosolic translocation of HMGB1 represents a key event in activating the autophagic process. Therefore, we pointed at elucidating if TERF2, altering the localization of HMGB1, would impact on autophagy. To this aim, HeLa cells

chronically silenced for TERF2 were transfected with EGFP-tagged LC3B (EGFP-LC3B) and the percentage of cells with EGFP-LC3B foci (LC3 puncta-positive cells) was quantified. Interestingly, IF experiments – then biochemically confirmed by WB analysis – demonstrated that the down-regulation of TERF2 promotes a significant increase in the percentage of EGFP-LC3B puncta-positive cells (Figure 3(a); Fig. S3A and S3B). In parallel, the autophagic role of TERF2 was also confirmed *in vivo*, by immunohistochemical experiments. As reported in the Figure 3(b), tumors originating from TERF2-silenced cells (shTERF2) showed a significative increase of LC3 staining in comparison with the tumors originated from control cells (shSCR).

Conversely to silencing experiments, the overexpression of TERF2 was found to impair the activation of autophagy mediated by nutrient starvation (Fig. S3C). For completeness, the role of TERF2 in autophagy was also evaluated in other cancer cell lines and under different pro-autophagic stimuli. The obtained data demonstrated that silencing of TERF2 promotes autophagy also in HT1080, a fibrosarcoma cell line, and HCT116, a colorectal cancer cell line (Fig. S3D-S3F), and that its effect also occurred upon rapamycin

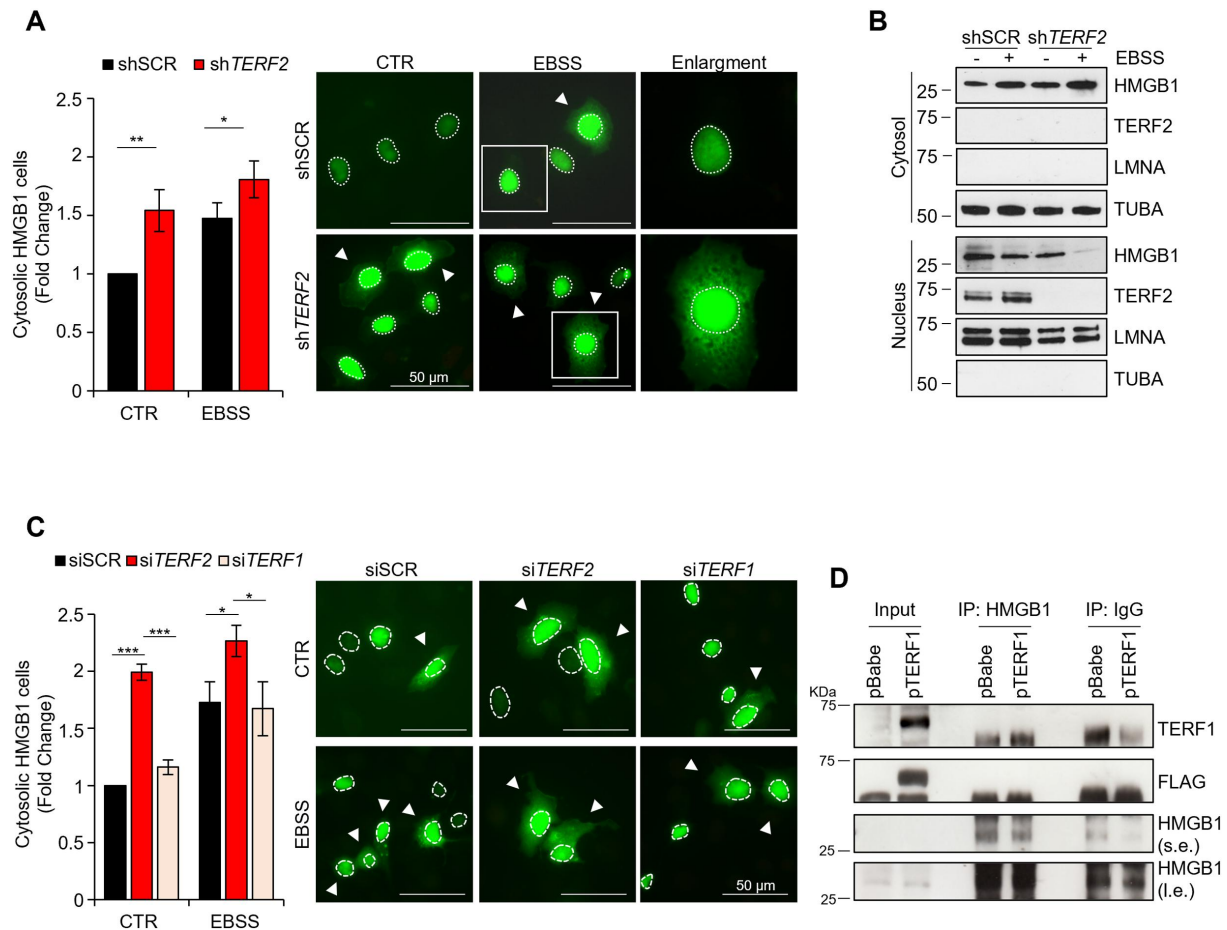


Figure 2. TERF2 silencing promotes the cytosolic translocation of HMGB1. (A) HeLa cells stably silenced for TERF2 (shTERF2), and their respective control (shSCR), were transfected with the recombinant protein EGFP-HMGB1 for 24 h, starved with EBSS for 1 h and finally processed for fluorescence assay. *Left panel.* Percentage of cells with cytosolic HMGB1 evaluated on total GFP-positive cells. *Right panel.* Representative images acquired by deconvolution microscopy (magnification 63X). Arrowheads indicate cells showing HMGB1 cytosolic localization. (B) Western blot analysis of HMGB1 protein levels in cytosolic (25 μ g) and nuclear extracts (5 μ g) obtained from HeLa shSCR and shTERF2 cells subjected or not to EBSS starvation for 1 h. α -TUBA and LMNA protein levels were used as controls of protein extraction and loading. TERF2 protein levels were used as control of protein silencing. (C) *Left panel.* Quantitative analysis showing the percentage of cells with cytosolic HMGB1 performed in HeLa cells silenced for TERF2 (siTERF2), TERF1 (siTERF1) and their control counterpart (siSCR). *Right panel.* Representative images acquired by deconvolution microscopy (magnification 63X). Arrowheads indicate cells showing HMGB1 cytosolic localization (D) IP experiment performed in HeLa cells subjected (pTERF1) or not (pBabe) to stable overexpression of FLAG-TERF1. IP were performed by using an antibody against HMGB1. The amount of TERF1 immunoprecipitated by HMGB1 antibody was evaluated by western blot analysis using both the antibody against TERF1 and that against FLAG. Evaluation of HMGB1 protein levels was used as internal control. All the histograms represent the mean values \pm S.D. of three independent experiments. * $p < 0.05$; ** $p < 0.01$; *** $p < 0.001$.

treatment and hypoxia (Fig. S3G-S3I), indicating that the role played by TERF2 on autophagy is independent from tumor histotype and the stimulus used.

To gain deeper insight into the role of TERF2 in the autophagic process, cells stably silenced for TERF2 were transfected with the mRFP-EGFP tandem fluorescence-tagged LC3B construct (ptf-LC3) to monitor the autophagic flux. IF experiments evidenced, together with an increase of autophagosomes (yellow-fluorescence structures), the presence of ALs (red-fluorescence structures), definitively indicating that silencing of TERF2 promotes an increase in the autophagic flux (Figure 3(c)).

Because TERF2-dependent activation of DNA damage response (DDR) is known to promote the autophagic process through the release of damaged DNA fragments within the cytosol [34], an eventual contribution of the DNA damage deriving from the silencing of TERF2 cannot be neglected.

For this reason, analysis of DDR pathway was performed in our model. In line with previous data published from our and other laboratories [16,35], it was found that, conversely to the acute silencing of TERF2, chronic depletion of the protein did not induce a persistent DNA damage, that – as evidenced by IF and WB analyses – is not detectable either at genomic or telomeric level (Fig. S4A-S4D).

Finally, to definitively demonstrate that the autophagic role of TERF2 is dependent on the shuttling of HMGB1, cells chronically silenced for TERF2 were treated with inflachromene (ICM), a specific inhibitor of the cytosolic translocation of HMGB1 [36] (Fig. S4E). As shown in the Figure 3(a), ICM treatment completely reverts the autophagic activity of TERF2 under both basal condition and EBSS-stimulation. To confirm and reinforce the obtained results, the pharmacological approach was paralleled by genetic experiments based on the silencing of HMGB1 (siHMGB1), as well as ATG7 (autophagy related 7), an

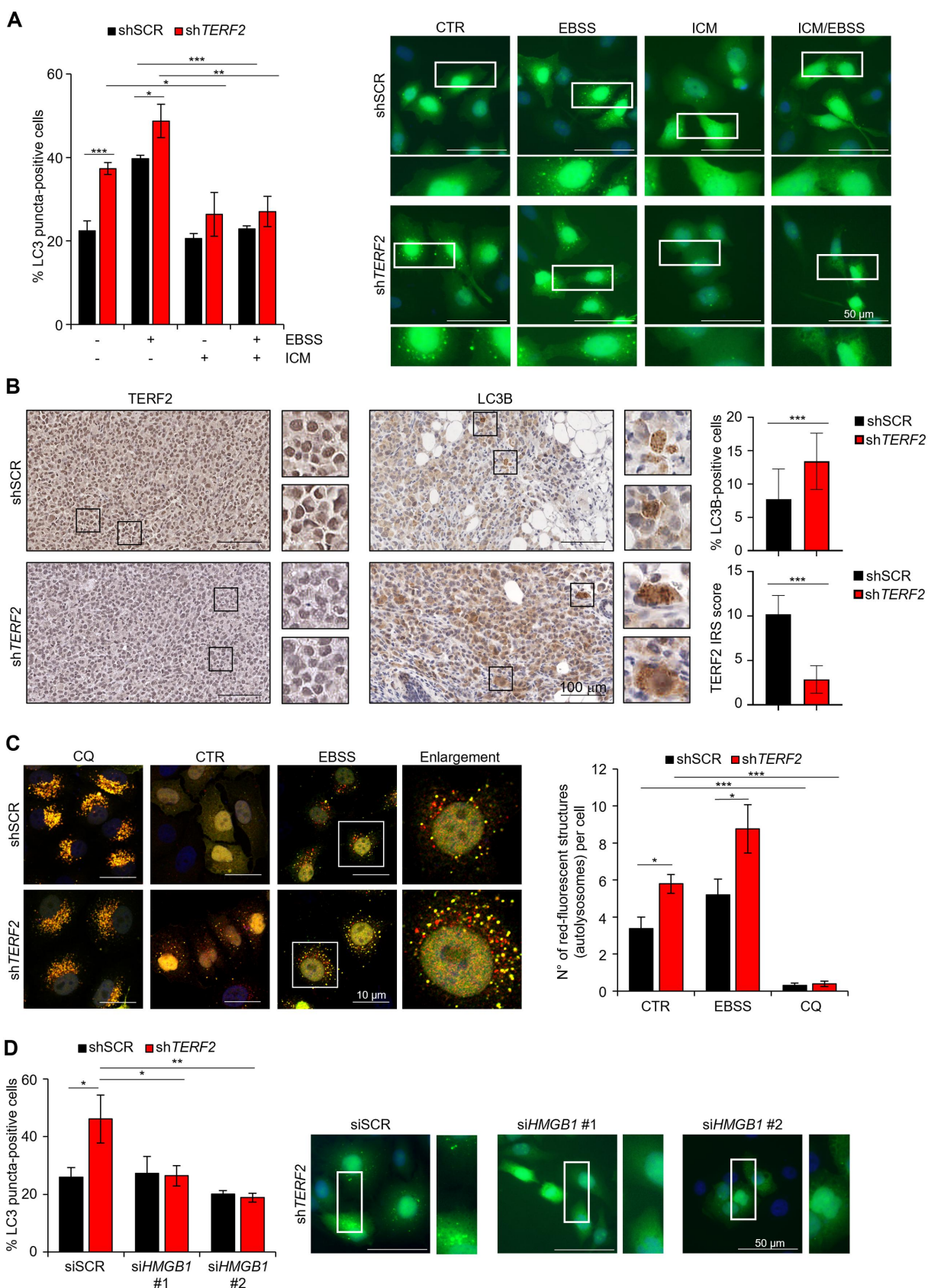


Figure 3. TERF2 regulates autophagy in a HMGB1-dependent manner. (A) HeLa cells silenced (shTERF2) or not (shSCR) for TERF2 were transfected with EGFP-LC3B for 24 h, treated with 25 μ M Inflachromene (ICM) for 6 h and subjected to EBSS starvation during the last 1 h. The autophagic process was evaluated by the quantitative analysis of punctate vesicular structures by fluorescence experiments. *Left panel.* The histogram represents the percentage of LC3 puncta-positive cells on total GFP-positive cells. *Right panel.* Representative images acquired by deconvolution microscopy (magnification 63X). Specific enlargements are shown. (B) IHC analyses of TERF2 and LC3B. *Left panel.* Representative images of TERF2 and LC3B immunostained sections of primary tumor established from tumor cells silenced (shTERF2) or not (shSCR) for TERF2. *Right panel.* Quantification of LC3 (expressed as the percentage of LC3B-positive cells) and TERF2 expression (expressed as Immunoreactive Score, IRS). Thirty fields for condition were analyzed. (C) HeLa shSCR and shTERF2 cells were transiently transfected with mRFP-EGFP-LC3B (ptf-LC3) and subjected to

enzyme playing a central role in autophagosome biogenesis [37]. The obtained results evidenced that down-regulation of these proteins abrogates the pro-autophagic activity of TERF2 silencing (Figure 3(d); Fig. S4F-S4H). In parallel, the expression of the HMGB1^{C106S} – a mutant that, constitutively localizing in the cytosol, promotes autophagy independently from stimulation [29] – reverts the inhibitory effect of TERF2 overexpression on autophagy (Fig. S4I). Altogether, these results clearly indicate that TERF2 regulates autophagy by controlling the translocation of HMGB1 into the cytosol.

TERF2 affects HMGB1-localization by regulating the redox status of tumor cells

As reported in the literature, HMGB1 is a redox-sensitive protein that needs to be oxidized to translocate in the cytosol and activate autophagy [28,30]. Based on this knowledge, we questioned if TERF2, besides sequestering HMGB1 into the nucleus, might also influence the protein shuttling of HMGB1 by altering the redox status of the cells. To address this point, the levels of reduced (GSH) and oxidized (GSSG) glutathione were evaluated in cells silenced or not for TERF2. Interestingly, data analysis evidenced a significant decrease in GSH:GSSG ratio (Figure 4(a)). Moreover, fluorescence-activated cell sorting (FACS) performed with two different probes – dihydroethidium (DHE) and 2',7'-dichlorofluorescein diacetate (DCFDA) – evidenced that the accumulation of reactive oxygen species (ROS), observed upon EBSS stimulation, is exacerbated by TERF2 depletion (Figure 4(b); Fig. S5A). Consistently with these data, silencing of TERF2 was found to promote an increase in the cellular levels of 8-hydroxy-2'-deoxyguanosine (8-OHdG), a marker of oxidatively damaged DNA [38], both *in vitro* and *in vivo* (Fig. S5B and S5C). Altogether these data indicate that the down-regulation of TERF2 levels associates with an altered glutathione homeostasis and with a burst of oxidative stress.

To verify the involvement of intracellular redox state in the TERF2-dependent autophagy, cells were treated with the antioxidant N-acetylcysteine (NAC) before the EBSS starvation. Interestingly, pre-treatment with NAC, reducing ROS levels (Fig. S5D), impairs HMGB1 cytosolic translocation (Figure 4(c)), thus inhibiting cell autophagy (Figure 4(d)). In parallel with these experiments, TERF2-overexpressing cells (pTERF2), and their control counterpart (pBabe), were treated with hydrogen peroxide (H₂O₂), a potent inducer of oxidative stress [39], and cellular localization of HMGB1 was evaluated by IF experiments (Figure 4(e)). As expected, the treatment with H₂O₂ promotes cytosolic translocation of HMGB1 in the control cells, but this effect is impaired in the cells overexpressing TERF2. These results indicate that an excess of the telomeric

protein limits the response of HMGB1 to those pro-oxidant stimuli, that commonly trigger its cytosolic translocation.

Collectively these results indicate that TERF2 controls autophagy by regulating the cytosolic translocation of HMGB1 in two complementary ways: on one hand by holding the HMGB1 into the nucleus and, on the other hand, by affecting the cellular redox homeostasis (Figure 5).

Discussion

TERF2 – beyond its telomeric functions – plays a key role in cancer biology by promoting tumor formation and progression, two events that have been associated with immune-surveillance escape [14,15] and tumor angiogenesis [16,17]. At the molecular level, these telomere-independent functions derive from its ability to affect a plethora of molecular processes, including control of gene transcription [14,15,40–42], synthesis of ribosomal RNA [43], regulation of microRNAs' expression [18] and establishment of protein complexes [18,19,44].

In this work, we disclosed an additional role of TERF2 in controlling autophagy. In particular, our data demonstrated that the depletion of TERF2 promotes the autophagic process, a result that is in accordance with a recent study in which the authors correlated autophagy with the DDR deriving from TERF2 silencing in normal cells [34]. Despite TERF2 depletion is reported to activate DDR pathway, telomeres of certain cancer cell lines have been found to be resistant to a partial loss of the protein [15,35]. Here, in line with previous data obtained from our and other laboratories [16,35], we demonstrated that chronic depletion of TERF2 – conversely to its acute silencing – does not induce detectable levels of DNA damage in HeLa cells. This model offered us the unique opportunity to identify a previously unreported mechanism through which TERF2, in absence of DDR activation, can control autophagy.

In this context, analysis of autophagy evidenced that the downregulation of TERF2 induces the formation of both autophagosomes and ALs, indicating that the silencing of the telomeric protein promotes activation of the autophagic flux. Moreover, our data highlighted that pro-autophagic activity induced by TERF2 silencing is comparable with that induced by canonical pro-autophagic stimuli (*e.g.* nutrient starvation, hypoxia or rapamycin treatment), thus underlying the biological relevance of our findings. Finally, mirror experiments demonstrated that TERF2 overexpression, conversely to its silencing, plays an anti-autophagic role. Of note, opposite results obtained by modulating TERF2 protein in the two directions (up and down) demonstrated the specificity of TERF2 activity in regulating the autophagic process, thus strengthening our data. Nevertheless, the effect derived by

EBSS starvation. Autophagic flux was assessed by analyzing yellow- and red-fluorescence structures, indicating an accumulation of autophagosomes and autolysosomes, respectively. Treatment with the autophagic inhibitor chloroquine (CQ) at 12 μ M for 24 h was used as a positive control of autophagosome accumulation. *Left panel.* Confocal microscopy images of a representative experiment (63X magnification). *Right panel.* Quantitative analysis showing the average number of LC3 red-fluorescence puncta per cell. The histogram represents the mean \pm SEM of one representative experiment. (D) *Left panel.* Quantitative analysis of punctate vesicular structures in HeLa shSCR and shTERF2 transiently silenced (shHMGB1 #1 and #2) or not (siSCR) for HMGB1. *Right panel.* Representative images acquired by deconvolution microscopy (magnification 63X). Specific enlargements are shown. The histograms, when not specified, represent the mean values \pm S.D. of three independent experiments. **p* < 0.05; ***p* < 0.01; ****p* < 0.001, *****p* < 0.0001.

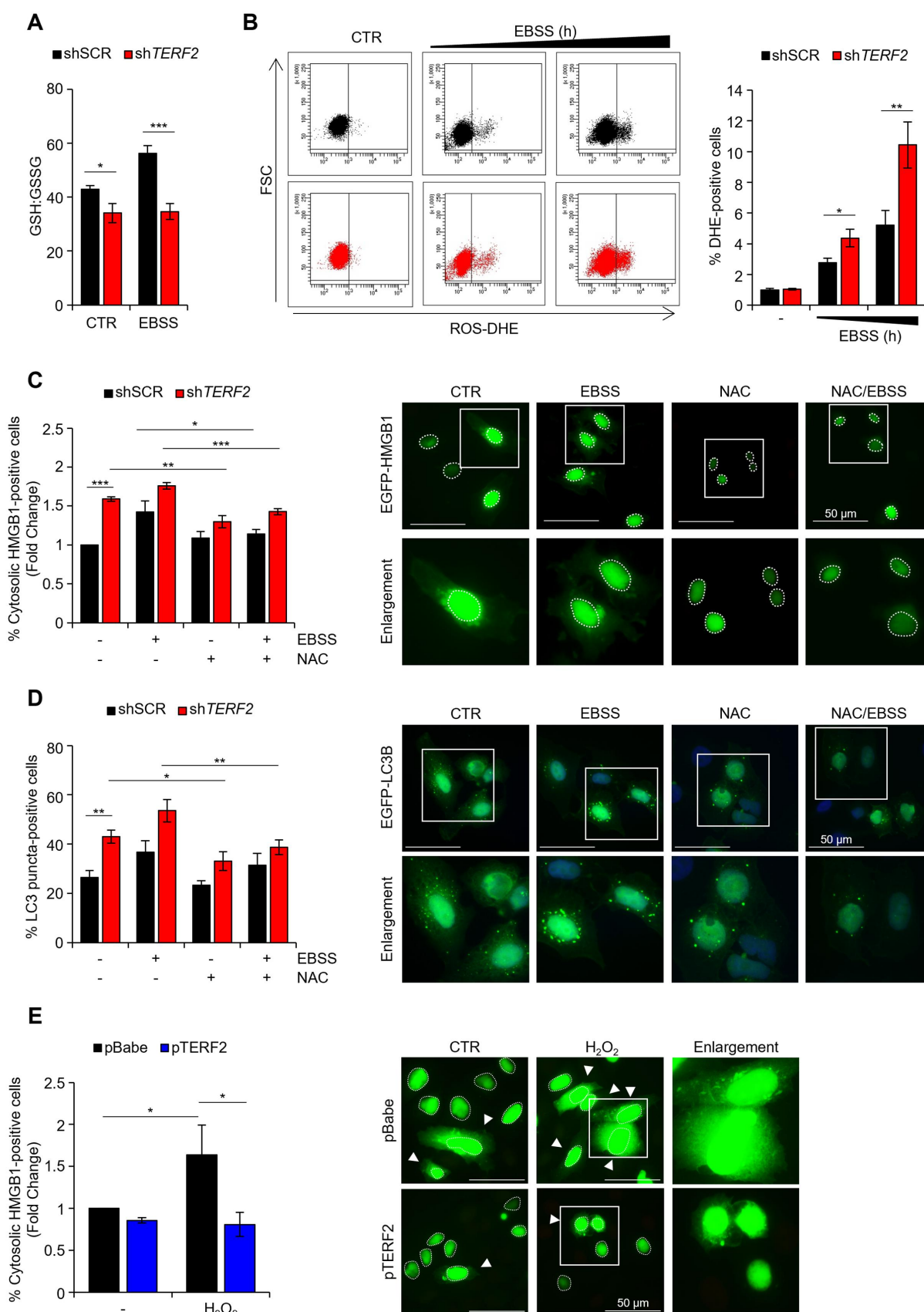


Figure 4. TERF2 regulates cytosolic translocation of HMGB1 altering the redox status of the cells. (A) HeLa cells stably silenced for TERF2 expression (shTERF2), and their respective control (shSCR), were treated with EBSS for 30 min and processed for the evaluation of GSH and GSSG intracellular levels by HPLC. The histogram shows the GSH:GSSG ratio. (B) FACS analysis of ROS-positive cells, detected with DHE, in HeLa shSCR and shTERF2 cells starved with EBSS for increasing times. *Left panel.* Representative images of FACS analysis. *Right panel.* Quantitative analysis of FACS experiments. (C) HeLa shSCR and shTERF2 were transfected with EGFP-HMGB1 for 24 h, pre-treated with the antioxidant NAC 5 mM for 3 h and starved with EBSS for the last 1 h. *Left panel.* Quantitative analysis showing the percentage of cells with cytosolic EGFP-HMGB1 on total GFP-positive cells. *Right panel.* Representative images acquired by deconvolution microscopy (magnification 63X). (D)

the up-regulation of TERF2 levels is evident only under pro-autophagic stimuli and this is reasonably due to the impossibility of appreciating a further decrease in the already low autophagic levels detectable in steady-state conditions.

Together with the clarification of the role of TERF2 in the autophagic process, we defined the molecular mechanism – complementary to DDR activation – through which TERF2 affects autophagy. Interestingly, the mechanistic part of this work comes from our recent study demonstrating that HMGB1, a multifunctional protein known to promote autophagy [30], localizes at telomeres [32]. By adopting complementary technical approaches based on both IF microscopy (e.g. colocalization experiments, PLA) and biochemistry (IP experiments, affinity-isolation assays), here we demonstrated that HMGB1 interacts with TERF2 in a DNA-dependent manner. Indeed, DNA digestion by DNase, as well as the overexpression of a TERF2 mutant unable to bind the DNA, determined a loss of the interaction between the two proteins. Interestingly, functional analysis of the discovered interaction revealed that cellular localization of HMGB1 is tightly dependent on the expression levels of TERF2. In particular, we demonstrated that the amount of cytosolic fraction of HMGB1 inversely correlates with the levels of TERF2 expression, an effect that is mainly due to the ability of TERF2 to sequester HMGB1 into the nucleus. This is in accordance with the literature data reporting that HMGB1 shuttles from the nucleus to the cytosol where it exerts its pro-autophagic activity [30]. However, as evidenced by our results, TERF2 activity is not limited to holding HMGB1 into the nucleus but it actively controls the protein localization by affecting the redox status of the cell, an event that finally impacts on HMGB1 translocation. Since our data evidenced oxidative DNA damage subsequent to the silencing of TERF2, we cannot exclude that this event – even if not accompanied by the phosphorylation of histone H2AX (γ H2AX) – could contribute to autophagy. Nevertheless, we demonstrated that TERF2 overexpression is able to counteract the cytosolic translocation of HMGB1 promoted by a potent inducer of oxidative stress like H_2O_2 , reinforcing the idea that TERF2, binding HMGB1, regulates the amount of telomere-free HMGB1. Notably, the molecular mechanism through which TERF2 influences the redox status of the cells remains to be clarified but, despite its general interest, it is out of the scope of this work.

The role of oncogenic proteins in autophagy is quite controversial; indeed, while some oncogenes, such as Ras, are reported to enhance the autophagic process, several others, such as the BCL2 family members, may select for cells with a reduced autophagic activity [45,46]. In this context, our data highlight TERF2 as a novel anti-autophagic oncogenic factor. Even if the reasons of the different behaviors of oncogenic proteins in autophagy have been not yet fully elucidated,

a possible explanation could rely on the complexity of the autophagic process that impacts, in a context-dependent manner, on oncogenesis and on the tumor response to anticancer treatments [47,48]. In particular, autophagy is reported to have a dual role in cancer, on one hand, by inhibiting early stages of tumor and, on the other hand, by playing a promoting activity in the later stages [23]. In accordance with its role in inhibiting autophagy, we can speculate that TERF2 can promote cell growth in the initial phases of tumorigenesis while, in advanced tumors, it can increase sensitivity of cancer cells to treatments, thus representing an Achilles's heel to take in advantage for counteracting the progression of the malignancy.

Materials and methods

Cells and culture conditions

HeLa, HCT116, HT1080 and U2OS human cell lines were purchased from American Type Culture Collection (ATCC, CCL-2, CCL-247, CCL-121 and HTB-96) and were cultured in Dulbecco's modified Eagle's medium (DMEM; EuroClone, ECM0728L), supplemented with L-glutamine, penicillin-streptomycin and 10% fetal bovine serum (FBS; Thermo Fisher Scientific/Gibco, 10,270–106), in a CO_2 -humidified incubator at $37^\circ C$.

Stable TERF2-overexpressing (pTERF2) and TERF2-silenced (shTERF2 #1 and shTERF2 #2, obtained by using two different short hairpin sequences directed against TERF2) cells, and their respective controls (pBabe and shSCR), were obtained as previously described [16].

Stable TERF1-overexpressing (pTERF1) cells were obtained by infecting the cells with amphotropic retroviruses generated into Phoenix packaging cells transfected with retroviral vectors, using the JetPEI reagent (Polyplus, 101–10 N), according to the manufacturer's instructions.

For transient overexpression of the wild-type (pTERF2) and the mutant (pTERF2 ΔC) forms of TERF2, HeLa cells were transfected for 48 h with the vectors pBabe-puro-MYC-TERF2 and pBabe-puro-MYC-TERF2 ΔC , respectively, using JetPEI reagent, according to the manufacturer's instructions. pBabe-puro empty vector was used as control. For transient silencing of TERF2 or TERF1, HeLa cells were transfected for 24 h with 100 nM of siTERF2 (Dharmacon, 5'-GCAGAAGUGGACUGUAGAAUU-3') or 50 nM of siTERF1 (OriGene Technologies, SR322000B), using INTERFERin reagent (Polyplus, 409–10), according to the manufacturer's instructions. A control short interfering RNA (Santa Cruz Biotechnology, sc-37,007) was used as control.

For the silencing of HMGB1 and ATG7, HeLa cells were transiently transfected for 48 h with 100 nM of siHMGB1 #1 (Santa Cruz Biotechnology, sc-37,982) or 40 nM of siHMGB1 #2 (Dharmacon, J-018981-08-0005) and 25 nM of siATG7

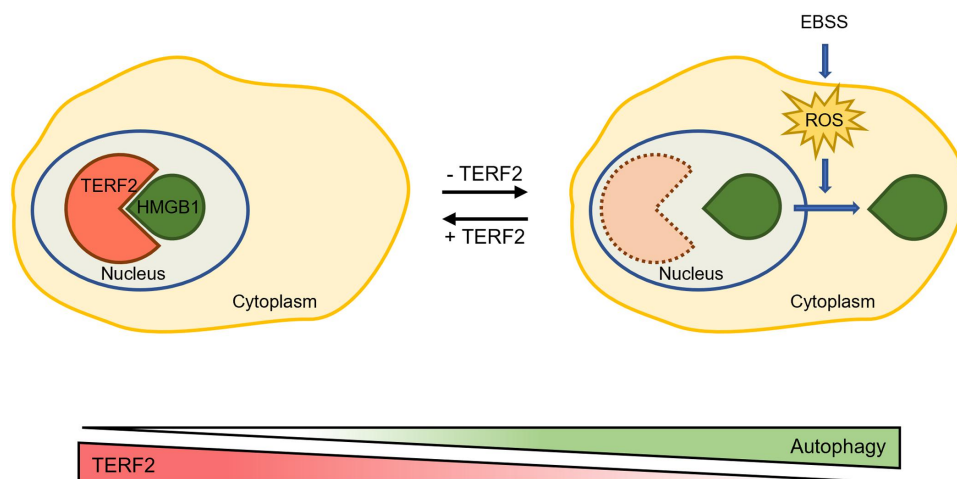


Figure 5. Schematic representation of the results. Cartoon summarizing the main findings of this work. *Left panel.* The interaction between TERF2 and HMGB1 occurring, in the nucleus, under steady-state conditions. *Right panel.* Schematization of the effects of TERF2 depletion on HMGB1 translocation.

(Sigma-Aldrich, 5'-ATGGAGAGCTCCTCAGCAGGC-3'), respectively, by using INTERFERin reagent, according to the manufacturer's instructions.

For the transient expression of EGFP-LC3B, mCherry-LC3B, mRFP-EGFP-LC3B (ptf-LC3), EGFP-HMGB1, the cells were transfected for 24 h by using JetPEI, according to the manufacturer's instructions. For the transient expression of EGFP-HMGB1^{C106S}, the cells were transfected for 48 h by using JetPEI, according to the manufacturer's instructions.

Reagents and treatments

For starvation experiments, cells were incubated in Earle's balanced salt solution (EBSS; BioWhittaker, BE10-502 F) for the indicated times.

HMGB1 inhibitor, inflachromene (ICM; Sigma-Calbiochem, 533,060), was dissolved in DMSO and used at 25 μ M for 6 h. Chloroquine (CQ; Sigma-Aldrich, St. Louis, Missouri, USA, C6628) was freshly dissolved in H₂O and used at a final concentration of 12 μ M for 24 h for fluorescence assays and 30 μ M for 3 h for WB applications. N-acetyl-L-cysteine (NAC; Sigma-Aldrich, A7250) was freshly dissolved in 12% NaOH 5 M and administered to cells at a concentration of 5 mM for 3 h as a pre-treatment. Rapamycin (Selleckchem, S1039) was dissolved in DMSO and used at a final concentration of 0.5 μ M for the indicated times. H₂O₂ was diluted in DMEM and used at a final concentration of 300 μ M for 10 min.

Hypoxic conditions were obtained using Forma Series II Water Jacket CO₂ Incubator (Thermo Fisher Scientific), set to 1% of oxygen.

Western blot

Western blot analysis was performed as previously reported [49]. Nuclear and cytosolic proteins extraction was performed using NE-PER Nuclear and Cytoplasmic Extraction Reagents

(Thermo Fisher Scientific, 78,835), according to the manufacturer's instructions.

The following primary antibodies were used: rabbit polyclonal antibody (pAb) anti-HMGB1 (Abcam, Ab18256); mouse monoclonal antibody (mAb) anti-TERF2/TRF2 4A794 (Millipore, 05-521); mouse mAb anti-MYC/cMyc (Santa Cruz Biotechnology, sc-40); mouse mAb anti-TUBA/ α Tubulin (Santa Cruz Biotechnology, sc-8035); mouse mAb anti-LMNA/lamin A/C (Santa Cruz Biotechnology, sc-7292); mouse mAb anti-TERF1/TRF1 (clone 4E4; Invitrogen, Carlsbad, California, USA, MA5-31,596); rabbit pAb anti-Flag (Sigma-Aldrich, F7425); rabbit pAb anti-CTCF (Diagenode, Belgium, C15410210-50); rabbit pAb anti-LC3B (Sigma-Aldrich, L7543); mouse mAb SQSTM1/p62 (clone D-3; Santa Cruz Biotechnology, sc-28,359); mouse mAb anti-HIF1A/HIF1 α (Clone 54/HIF-1 α ; BD Transduction Laboratories, San Jose, CA, USA, 610,959); rabbit mAb anti-Ser1981 p-ATM (Abcam, ab208775); rabbit pAb anti-Thr68 p-CHEK2/Chk2 (Cell Signaling Technology, 2661); mouse mAb anti-phospho-histone H2AX (γ H2AX; Millipore, 05-636); mouse mAb anti-ATG7 (Clone B-9; Santa Cruz Biotechnology, sc-376,212); mouse mAb anti-ACTB/ β -actin (Sigma-Aldrich, A5441).

The following secondary antibodies were used: goat anti-mouse (Bio-Rad, 1,706,516) or anti-rabbit immunoglobulin G (IgG)-horseradish peroxidase conjugated antibodies (Bio-Rad, 1,706,515).

Immunoprecipitation (IP)

Regarding IP experiments, nuclear cell extracts of HeLa cells were obtained by a sequential lysis with buffer A [10 mM HEPES pH 7.9 (Fisher scientific, BP299-100), 10 mM KCl (Sigma-Aldrich, 44,675), 0.1 mM EDTA (Sigma-Aldrich, E9884), 0.1 mM EGTA (Millipore, 324,628), 0.6% NP-40 (Millipore, 492,016), 1 mM DTT (Roche, 10,197,777,001) and 1 mM PMSF (Roche, P7626)] and buffer C [20 mM HEPES, pH 7.9, 400 mM NaCl (Sigma-Aldrich, S9888), 1 mM EDTA, 1 mM EGTA, 1 mM DTT and 1 mM PMSF], which resulted

respectively in cytosolic and nuclear fraction isolation. Protein concentration was determined by Pierce™ BCA Protein Assay Kit (Thermo Fisher Scientific, 23,225) and 700 µg of nuclear fraction were immunoprecipitated by using 4 µg of the indicated antibody and 50 µl of Dynabeads Protein A/G (Invitrogen, 10002D/10004D), according to manufacturer's instructions. The following primary antibodies were used for IP: mouse mAb anti-TERF2/TRF2 4A794 (Millipore, 05–521), rabbit pAb anti-HMGB1 (Abcam, Ab18256). IP with anti-normal mouse IgG (Santa Cruz Biotechnology, sc-2025) and anti-normal rabbit IgG (Santa Cruz Biotechnology, sc-3888) were used as respective negative controls.

Proximity Ligation Assay (PLA)

Cells were grown on gelatin-coated glass coverslips for 24 h, fixed in 4% formaldehyde in phosphate-buffered saline (PBS; EuroClone, ECB4004L) 1X for 10 min at room temperature (RT) and processed with Duolink® In Situ Red Starter Kit mouse/rabbit (Sigma-Aldrich, DUO92101), according to the manufacturer's instructions. The following primary antibodies were used: Mouse mAb anti-TERF2/TRF2 4A794 (Millipore, 05–521) and rabbit pAb anti-HMGB1 (Abcam, Ab18256).

Fluorescence signals were recorded by using a Leica DMIRE2 microscope equipped with a Leica DFC 350FX camera and elaborated by Leica FW4000 deconvolution software (Leica, Germany). The number of TERF2-HMGB1 PLA spots per cell were counted by visual inspection on the maximum projection resulting from multiple z-stack images and a total of 80 cells was considered.

Fluorescence microscopy

Cells were grown on glass coverslips, treated according to the experiment, fixed in 4% formaldehyde in PBS for 10 min at RT and permeabilized with 0.25% Triton X-100 (Sigma-Aldrich, 93,443) for 5 min at RT.

Concerning TERF2-HMGB1 colocalizations, HeLa and U2OS cells were subjected to co-immunofluorescence experiments. After fixation and permeabilization, cells were incubated with rabbit pAb anti-TERF2/TRF2 (Novus, Italy, NB110-57,130) and mouse mAb anti-HMGB1 (Santa Cruz Biotechnology, sc-135,809) for 2 h at RT. After three washes in PBS, cells were incubated with anti-rabbit IgG (H + L), F(ab')₂ Fragment (Alexa Fluor 488 Conjugate; Cell Signaling Technology, 4412S) and anti-mouse IgG (H + L), F(ab')₂ Fragment (Alexa Fluor 555 Conjugate; Cell Signaling Technology, 4409S) for 1 h at RT. Nuclei were stained with 4',6-diamidino-2-phenylindole (DAPI; Sigma-Aldrich, D9542).

To analyze the cellular levels of 8-OHdG, cells were processed for IF as reported above and incubated with the primary antibody mouse mAb anti-8-OHdG (clone 15A3; Santa Cruz Biotechnology, sc-66,036) at + 4°C overnight. Successively, the cells were incubated with anti-mouse IgG (H + L), F(ab')₂ Fragment (Alexa Fluor 555 conjugate) for 1 h at RT and the nuclei were stained with DAPI.

Cellular localization of HMGB1 was assessed by fluorescence microscopy analyses in cells transiently transfected with EGFP-HMGB1 for 24 h. Percentage of cells with cytosolic HMGB1 was evaluated on total GFP-positive cells. DAPI staining was used to exclude mitotic events from the analyses.

For autophagy experiments, cells were transiently transfected with EGFP-LC3B or mCherry-LC3B, treated according to the experimental settings and then processed for fluorescence microscopy. Autophagosome structure formation was detected by observing LC3B puncta in EGFP-LC3B- or mCherry-LC3B-expressing cells. For each experimental condition, at least 250 cells were counted; cells with more than 10 puncta were considered positive for autophagy. The results were represented as the percentage of autophagy-positive cells respect EGFP-LC3B or mCherry-LC3B expressing cells. Fluorescence signals were recorded by using a Leica DMIRE2 microscope equipped with a Leica DFC 350FX camera and elaborated by Leica FW4000 deconvolution software (Leica). Regarding the analysis of the autophagic flux, cells were transiently transfected with (ptf-LC3), as previously reported, treated with EBSS for 1 h or CQ for 3 h and processed for fluorescence. The formation of yellow- and red-fluorescence structures – indicating an accumulation of autophagosomes and autolysosomes, respectively – was evaluated. The number of LC3 red-fluorescence puncta per cell was quantified by using ImageJ Software.

In order to evaluate the DNA damage, immunofluorescence experiments were combined with telomeric FISH assays. After fixation and permeabilization, cells were blocked for 1 h with 3% BSA in PBS 1X and incubated with the mouse mAb anti-phospho-histone H2AX (γH2AX; Millipore, 05–636) overnight at 4°C. After two washes with 0.05% Triton X-100 in PBS 1X, the cells were incubated with the secondary antibody anti-mouse IgG (H + L), F(ab')₂ Fragment (Alexa Fluor 488 Conjugate) for 1 h at RT and then washed twice with PBS 1X. Successively, a Telomere DNA FISH was carried out as previously described [50]. Nuclei were stained with DAPI. For quantitative analysis of γH2AX positivity, at least 250 cells/condition were scored in triplicate. For Telomere-Induced Foci (TIFs) analysis, at least 25 γH2AX-positive cells on a single plane were scored. Cells with at least four telomere-γH2AX colocalization spots were considered TIF-positive. Fluorescence signals were recorded with Zeiss Laser Scanning Microscope 510 Meta (63X magnification) (Zeiss, Germany).

In vivo experiments

For *in vivo* experiments, NSG (NOD.Cg-PrkdcSCID IL-2 R null) female mice (Charles River Laboratories, strain 614) were orthotopically injected with 1×10^6 MDA-MB-231 cells silenced (shTERF2) or not (shSCR) for TERF2. When tumors reached a volume of about 300 mm³, mice were sacrificed and primary tumors underwent to immunohistochemical analysis.

Mice were maintained in a barrier facility on high-efficiency particulate air HEPA-filtered racks and received food and water ad libitum.

Immunohistochemistry (IHC)

The formalin-fixed and paraffin-embedded tissue blocks were sectioned (2 μ m) and subjected to deparaffinization, rehydration and antigen retrieval by PT Link (Agilent, PT10126), at low or high pH as suggested by the primary antibody data-sheets used. Endogenous peroxidase was blocked for 10 min with a peroxidase blocking solution (Agilent Dako, S2023) and, successively, nonspecific antibody binding was blocked for 20 min with protein blocking buffer (Agilent Dako, X0909). Tissue sections were immunostained for 1 h at RT with anti-TERF2/TRF2 rabbit polyclonal (1:500), anti-8-OHdG mouse monoclonal (1:800), anti-LC3B rabbit monoclonal (AbCam, EPR21234, 1:100) and then were covered for 30 min at RT with Dako EnVision™ FLEX /HRP (EnVision™ FLEX; Agilent, K8023). The signal was developed by using DAB detection kit (Agilent Dako, GV825), then sections were counterstained with Mayer's Hematoxylin (Agilent Dako, S3309). Finally, slides were washed, dehydrated with increasing alcohol and xylene and mounted with Eukitt (Sigma-Aldrich, 03989). Immunostaining results were recorded as percentage of positive cells or immunoreactive score (IRS, staining intensity per percentage of positive cells).

Reactive oxygen species (ROS) production

Stable TERF2 interfered HeLa cells, and their control counterpart, were starved with EBSS for the indicated times, harvested, washed in PBS 1X and stained for 30 min at 37°C with 25 μ M of dihydroethidium (DHE; Thermo Fisher Scientific, D1168) or 2',7'-dichlorofluorescein diacetate (DCFDA; Thermo Fisher Scientific, D399) dissolved in DMEM without FBS. About 20,000 events were acquired by using BD FACSCelesta™ C6 flow cytometer (BD Biosciences), gated using forward scatter and side scatter to exclude cell debris and analyzed with BD FACSDiva Software (BD Biosciences).

GSH:GSSG measurement

GSH and GSSG intracellular levels were evaluated as previously reported [51].

Statistics

Experiments were replicated three times and the data were expressed as means \pm standard deviation (SD). GraphPad Prism 6 was used for the statistical analysis and the differences between groups were analyzed by the unpaired Student's t-test. Differences were considered statistically significant for * $p < 0.05$; ** $p < 0.01$; *** $p < 0.001$; **** $p < 0.0001$.

Acknowledgments

We would like to thank Dr Eleonora Principalli and Dr Enrico Desideri for their technical support. We are very grateful to Professor Guido Kroemer (Sorbonne Université, Paris, France) for kindly giving us the recombinant protein EGFP-HMGB1, Professor George Hoppe (Cole Eye Institute, Cleveland Clinic, Cleveland, Ohio, USA) for EGFP-HMGB1 C106S, Professor Francesco Cecconi (Università di Roma Tor Vergata, Rome, Italy)

for the mCherry-LC3B and Dr Donatella Del Bufalo (IRCCS - Regina Elena National Cancer Institute, Rome, Italy) for the ptf-LC3B and EGFP-LC3B constructs. This work was supported by Funds Ricerca Corrente 2022 from Italian Ministry of Health and by Italian Association for Cancer Research (AIRC) under IG 2018 - ID. 21579 project - P.I. Biroccio Annamaria.

Disclosure statement

The authors report there are no competing interests to declare

Funding

This work was supported by the Italian Association for Cancer Research [21579];Ricerca Corrente 2022 from Italian Ministry of Health;

Data availability statement

The data that support the findings of this study are openly available at <https://gbox.garr.it/garrbox/index.php/s/pz4uKeqEt6vwcar>.

Ethics approval and consent to participate

All animal procedures were in compliance with the national and international directives (D.L. 4 March 2014, no. 26; directive 2010/63/EU of the European Parliament and European Council; Guide for the Care and Use of Laboratory Animals, U.S. National Research Council, 2011; Animal Research guidelines Reporting of *In Vivo* Experiments (ARRIVE) guidelines) and approved by the Italian Ministry of Health (authorization n. 607/2019-PR, released on 07-08-2019).

References

- [1] De Lange T. Shelterin-mediated telomere protection. *Annu Rev Genet.* 2018;52(1):223–247.
- [2] Feuerhahn S, Chen LY, Luke B, et al. No DDRama at chromosome ends: TRF2 takes centre stage. *Trends Biochem Sci.* 2015;40(5):275–285.
- [3] Pal D, Sharma U, Singh SK, et al. Over-expression of telomere binding factors (TRF1 & TRF2) in renal cell carcinoma and their inhibition by using SiRNA induce apoptosis, reduce cell proliferation and migration invitro. *PLoS ONE.* 2015;10(3):e0115651. Epub ahead of print.
- [4] Nakanishi K, Kawai T, Kumaki F, et al. Expression of mRNAs for telomeric repeat binding factor (TRF)-1 and TRF2 in atypical adenomatous hyperplasia and adenocarcinoma of the lung. *Clin Cancer Res.* 2003;9(3):1105–1111.
- [5] Diehl MC, Idowu MO, Kimmelshue KN, et al. Elevated TRF2 in advanced breast cancers with short telomeres. *Breast Cancer Res Treat.* 2011;127(3):623–630.
- [6] Chen W, Wang Y, Li F, et al. Expression of telomere repeat binding factor 1 and TRF2 in prostate cancer and correlation with clinical parameters. *Biomed Res Int.* 2017; Epub ahead of print. DOI:10.1155/2017/9764752.
- [7] Dong W, Wang L, Chen X, et al. Upregulation and CpG island hypomethylation of the TRF2 gene in human gastric cancer. *Dig Dis Sci.* 2010;55(4):997–1003.
- [8] Muñoz P, Blanco R, Flores JM, et al. XPF nuclease-dependent telomere loss and increased DNA damage in mice overexpressing TRF2 result in premature aging and cancer. *Nat Genet.* 2005;37(10):1063–1071.
- [9] Biroccio A, Rizzo A, Elli R, et al. TRF2 inhibition triggers apoptosis and reduces tumorigenicity of human melanoma cells. *Eur J Cancer.* 2006;42(12):1881–1888.
- [10] Mai M E, Wagner KD, Michiels JF, et al. The telomeric protein TRF2 regulates angiogenesis by binding and activating the PDGFR β promoter. *Cell Rep.* 2014;9(3):1047–1060.

- [11] Bai Y, Lathia JD, Zhang P, et al. Molecular targeting of TRF2 suppresses the growth and tumorigenesis of glioblastoma stem cells. *Glia*. 2014;62(10):1687–1698.
- [12] Yang D, Xiong Y, Kim H, et al. Human telomeric proteins occupy selective interstitial sites. *Cell Res*. 2011;21(7):1013–1027.
- [13] Simonet T, Zaragosi LE, Philippe C, et al. The human TTAGGG repeat factors 1 and 2 bind to a subset of interstitial telomeric sequences and satellite repeats. *Cell Res*. 2011;21(7):1028–1038.
- [14] Cherfils-Vicini J, Iltis C, Cervera L, et al. Cancer cells induce immune escape via glycoalkaloid changes controlled by the telomeric protein TRF 2. *EMBO J*. 2019;38(11). Epub ahead of print. DOI:10.15252/embj.2018100012.
- [15] Biroccio A, Cherfils-Vicini J, Augereau A, et al. TRF2 inhibits a cell-extrinsic pathway through which natural killer cells eliminate cancer cells. *Nat Cell Biol*. 2013;15(7):818–828.
- [16] Zizza P, Dinami R, Porru M, et al. TRF2 positively regulates SULF2 expression increasing VEGF - A release and activity in tumor microenvironment. *Nucleic Acids Res*. 2019;47(7):3365–3382.
- [17] Dinami R, Porru M, Amoreo CA, et al. TRF2 and VEGF-A: an unknown relationship with prognostic impact on survival of colorectal cancer patients. *J Exp Clin Cancer Res*. 2020;39(1):111.
- [18] Dinami R, Petti E, Porru M, et al. TRF2 cooperates with CTCF for controlling the oncomiR-193b-3p in colorectal cancer. *Cancer Lett*. 2022;533:215607.
- [19] Kim H, Lee OH, Xin H, et al. TRF2 functions as a protein hub and regulates telomere maintenance by recognizing specific peptide motifs. *Nat Struct Mol Biol*. 2009;16(4):372–379.
- [20] Mizushima N, Levine B, Cuervo AM, et al. Autophagy fights disease through cellular self-digestion. *Nature*. 2008;451(7182):1069–1075.
- [21] Deng Z, Li X, Ramirez MB, et al. Selective autophagy of AKAP11 activates cAMP/PKA to fuel mitochondrial metabolism and tumor cell growth. *Proc Natl Acad Sci U S A*. 2021;118(14). Epub ahead of print. DOI:10.1073/pnas.2020215118.
- [22] Levine B, Kroemer G. Autophagy in the pathogenesis of disease. *Cell*. 2008;132(1):27–42.
- [23] Chavez-Dominguez R, Perez-Medina M, Lopez-Gonzalez JS, et al. The double-edge sword of autophagy in cancer: from tumor suppression to pro-tumor activity. *Front Oncol*. 2020 October 7;10. Epub ahead of print. DOI:10.3389/fonc.2020.578418.
- [24] Chang H, Zou Z. Targeting autophagy to overcome drug resistance: further developments. *J Hematol Oncol*. 2020;13(1):159.
- [25] Galluzzi L, Baehrecke EH, Ballabio A, et al. Molecular definitions of autophagy and related processes. *EMBO J*. 2017;36(13):1811–1836.
- [26] Sun X, Tang D. HMGB1-dependent and -independent autophagy. *Autophagy*. 2014;10(10):1873–1876.
- [27] Goodwin GH, Sanders C, Johns EW. A new group of chromatin-associated proteins with a high content of acidic and basic amino acids. *Eur J Biochem*. 1973;38(1):14–19.
- [28] Yu Y, Tang D, Kang R. Oxidative stress-mediated HMGB1 biology. *Front Physiol*. 2015;6. Epub ahead of print. DOI:10.3389/fphys.2015.00093.
- [29] Tang D, Kang R, Livesey KM, et al. Endogenous HMGB1 regulates autophagy. *J Cell Biol*. 2010;190(5):881–892.
- [30] Chen R, Kang R, Tang D. The mechanism of HMGB1 secretion and release. *Exp Mol Med*. 2022;54(2):91–102.
- [31] Kwak MS, Rhee WJ, Lee YJ, et al. Reactive oxygen species induce Cys106-mediated anti-parallel HMGB1 dimerization that protects against DNA damage. *Redox Biol*. 2021;40:101858.
- [32] Amato J, Cerofolini L, Brancaccio D, et al. Insights into telomeric G-quadruplex DNA recognition by HMGB1 protein. *Nucleic Acids Res*. 2019;47(18):9950–9966.
- [33] Bower BD, Griffith JD. TRF1 and TRF2 differentially modulate Rad51-mediated telomeric and Nontelomeric displacement loop formation in Vitro. *Biochemistry*. 2014;53(34):5485–5495.
- [34] Nassour J, Radford R, Correia A, et al. Autophagic cell death restricts chromosomal instability during replicative crisis. *Nature*. 2019;565(7741):659–663.
- [35] Takai KK, Hooper S, Blackwood S, et al. In vivo stoichiometry of shelterin components. *J Biol Chem*. 2010;285(2):1457–1467.
- [36] Kim YH, Kwak MS, Shin JM, et al. Inflachromene inhibits autophagy through modulation of Beclin 1 activity. *J Cell Sci*. 2018 February;131(4). Epub ahead of print. DOI:10.1242/jcs.211201.
- [37] Komatsu M, Waguri S, Ueno T, et al. Impairment of starvation-induced and constitutive autophagy in Atg7-deficient mice. *J Cell Biol*. 2005;169(3):425–434.
- [38] Valavanidis A, Vlachogianni T, Fiotakis C. 8-hydroxy-2'-deoxyguanosine (8-OHdG): a critical biomarker of oxidative stress and carcinogenesis. *J Environ Sci Health C Environ Carcinog Ecotoxicol Rev*. 2009;27(2):120–139.
- [39] Ransy C, Vaz C, Lombès A, et al. Use of H2O2 to cause oxidative stress, the catalase issue. *Int J Mol Sci*. 2020 November 30;21(23):9149. Epub ahead of print.
- [40] Ye J, Renault VM, Jamet K, et al. Transcriptional outcome of telomere signalling. *Nat Rev Genet*. 2014;15(7):491–503.
- [41] Hussain T, Saha D, Purohit G, et al. Transcription regulation of CDKN1A (p21/CIP1/WAF1) by TRF2 is epigenetically controlled through the REST repressor complex. *Sci Rep*. 2017;7(1):11541.
- [42] Mukherjee AK, Sharma S, Bagri S, et al. Telomere repeat-binding factor 2 binds extensively to extra-telomeric G-quadruplexes and regulates the epigenetic status of several gene promoters. *J Biol Chem*. 2019;294(47):17709–17722.
- [43] Yuan F, Xu C, Li G, et al. Nucleolar TRF2 attenuated nucleolus stress-induced HCC cell-cycle arrest by altering rRNA synthesis. *Cell Death Dis*. 2018;9(5):518.
- [44] Rizzo A, Iachettini S, Salvati E, et al. SIRT6 interacts with TRF2 and promotes its degradation in response to DNA damage. *Nucleic Acids Res*. 2017;45(4):1820–1834.
- [45] Elgendy M, Sheridan C, Brumatti G, et al. Oncogenic Ras-induced expression of Noxa and Beclin-1 promotes autophagic cell death and limits clonogenic survival. *Mol Cell*. 2011;42(1):23–35.
- [46] Pattingre S, Levine B. Bcl-2 inhibition of autophagy: a new route to cancer? *Cancer Res*. 2006;66(6):2885–2888.
- [47] Panda PK, Mukhopadhyay S, Das DN, et al. Mechanism of autophagic regulation in carcinogenesis and cancer therapeutics. *Semin Cell Dev Biol*. 2015;39:43–55.
- [48] Maiuri MC, Tasdemir E, Criollo A, et al. Control of autophagy by oncogenes and tumor suppressor genes. *Cell Death Differ*. 2009;16(1):87–93.
- [49] Iachettini S, Triscuoglio D, Rotili D, et al. Pharmacological activation of SIRT6 triggers lethal autophagy in human cancer cells. *Cell Death Dis*. 2018;9(10). Epub ahead of print. DOI:10.1038/s41419-018-1065-0.
- [50] Petti E, Buemi V, Zappone A, et al. SFPQ and NONO suppress RNA:DNA-hybrid-related telomere instability. *Nat Commun*. 2019;10(1):1001.
- [51] Ciccarone F, Di Leo L, Lazzarino G, et al. Aconitase 2 inhibits the proliferation of MCF-7 cells promoting mitochondrial oxidative metabolism and ROS/FoxO1-mediated autophagic response. *Br J Cancer*. 2020;122(2):182–193.